International Journal of Innovative Research and Reviews, 10(1) 11-20

International Journal of Innovative Research and Reviews
ISSN: 2636-8919
Website: www.injirr.com

RESEARCH ARTICLE

Hydrogeochemistry, Petrography, and Groundwater Quality in the Waru–Apo Area (Abuja FCT, Nigeria)

Hairat Abubakar BANARU*[1], Benson Shedrach JATAU[1], Ishak Yau TANKO[1], Abdulmalik SADIQ

[1] *Department of Geology and Mining, Nasarawa State University, Keffi, Nigeria*

* *Corresponding author E-mail: hairatbanaru@hotmail.com*

ARTICLE INFO

Received : 01.19.2026
Accepted : 03.26.2026
Published : 07.15.2026

Keywords:
Abuja
Groundwater quality
Hydrogeochemistry
Heavy metals
Petrography
Pollution indices

ABSTRACT

The Waru–Apo area of the Federal Capital Territory (FCT), Abuja, lies at the intersection of two environmental challenges: a fractured crystalline basement aquifer with negligible primary porosity and prolonged contamination from unmanaged abattoir waste disposal. Because residents depend predominantly on hand-dug wells and shallow boreholes for domestic water, groundwater quality is of critical public health importance. This study integrates geological mapping, thin-section petrography, X-ray fluorescence (XRF) soil geochemistry, and atomic absorption spectrophotometry (AAS) groundwater analysis to characterize the lithological and hydrogeochemical framework of the area and evaluate the extent of heavy metal contamination. Twenty-two groundwater samples were collected from eleven locations, with paired samples analyzed separately for major anions and cations/metals. Four lithological units, i.e., migmatite, granite gneiss, biotite gneiss, and anatectic granite were identified. Mineral weathering processes, including plagioclase hydrolysis, biotite and sulphide oxidation, and ion exchange along fracture surfaces, control the dominant Na–SO_4 and Na–Mg–SO_4 hydrochemical facies, as confirmed by Gibbs, Durov, and Schoeller diagrams. Cadmium concentrations ranged from 0.034 to 0.121 mg/L, exceeding the WHO and NSDWQ guideline value of 0.003 mg/L at all sampling sites by factors of 11–40. Chromium and lead exceeded permissible limits at four sites each. Nemerow's Pollution Index classified all sites as severely polluted by cadmium (11.3–40.3). Soil chromium reached 842 ppm near the abattoir waste disposal area, while a strong positive correlation ($r = 0.82$, $p = 0.003$) between soil and groundwater chromium confirmed active contaminant leaching. Immediate groundwater protection, improved waste management, deeper borehole development, and routine groundwater monitoring are recommended.

Contents

Cite this article Banaru HA, Jatau BS, Tanko IY, Sadiqq A. Hydrogeochemistry, Petrography, and Groundwater Quality in the Waru–Apo Area (Abuja FCT, Nigeria). *International Journal of Innovative Research and Reviews (INJIRR)* (2026) 10(1) 11-20
Link to this article: http://www.injirr.com/article/view/258

1. Introduction

Crystalline basement terrains present a distinctive groundwater management challenge that sedimentary aquifer environments do not. Where a sandstone or limestone aquifer stores water in predictable intergranular pore space or karst conduits with measurable matrix permeability, a basement aquifer holds and transmits water almost entirely through fractures, joints, and the weathered regolith that accumulates above the fresh bedrock surface. That fracture system is efficient, well-connected, and essentially unfiltered: contaminants introduced at the surface travel rapidly downward to the water table and laterally in the direction of hydraulic gradient, with minimal retardation by clay mineral adsorption or organic matter complexation [1, 2]. In a community where those fractures are the only drinking water supply, and where a major waste-generating facility sits directly in the recharge zone above those fractures, the exposure risk is direct and continuous.

The Waru–Apo area of Abuja FCT is precisely such a community. Located within the crystalline Precambrian Basement Complex of north-central Nigeria, the area hosts a dense and growing residential population alongside one of the FCT's major abattoir operations. Blood, visceral waste, bone material, and the carbonaceous residues of vehicle tires burned during carcass singeing are discharged onto the ground surface with no containment infrastructure. The soils beneath and downslope of the abattoir compound receive this loading continuously through the wet season, and the fractured basement aquifer beneath receives whatever the vadose zone transmits downward. Despite this configuration, no integrated geological and hydrogeochemical assessment of the area had been published prior to this study.

The scientific basis for concern is well established in the literature. Emenike et al. [3] demonstrated in southwestern Nigeria basement terrain that heavy metal enrichment in groundwater was positively correlated with proximity to unlined waste disposal areas, confirming surface leaching as the dominant transfer mechanism. Elemile et al. [4] further confirmed that abattoir effluent in Nigerian urban settings elevates NH_3 and dissolved heavy metal concentrations beyond permissible limits, with cadmium exceedances of an order of magnitude common in unregulated operations. In a northern Nigeria context directly analogous to the present study, the combination of fractured basement geology, shallow well depths, and wet-season recharge pulses has been shown to create episodic but severe contamination events, with dry-season sampling consistently reflecting peak heavy metal concentrations.

In the regional West African context, chromium from hide-processing residues and cadmium from tire-burning have been identified as heavy metals of greatest public health concern in peri-urban abattoir settings. Alloway [5] and Reimann and Caritat [6] provide the geochemical basis for this concern: cadmium is highly soluble under acidic conditions, bioaccumulates in renal tissue, and is classified as a Group 1 human carcinogen by the International Agency for Research on Cancer. The FCT context adds further urgency — rapid population growth, limited piped water infrastructure, and the political profile of Abuja as a modern planned capital have created a situation where informal settlements and unregulated industries coexist with an aquifer that hundreds of thousands of people depend upon.

The hydrogeochemical framework for interpreting major ion chemistry in basement aquifers is provided by the diagrammatic methods of Gibbs [7], Piper [8], and Schoeller, as applied in numerous West African and global basement studies ([9, 10]; Rajmohan & Elango, 2004; Singh et al., 2017). The thermodynamic controls on heavy metal mobility, particularly the pH dependence of Cd^{2+}, Pb^{2+}, and Cr speciation, are documented in Appelo and Postma [11] and Hem [12]. The pollution index framework applied in this study (namely the Contamination Factor, Pollution Load Index [13], and Nemerow's Pollution Index [14]) represents the current methodological consensus for comprehensive groundwater quality characterization in contaminated basement settings, including the recognized limitation of the PLI's geometric mean structure in single-metal-dominated scenarios.

This study addresses the knowledge gap in the Waru–Apo area through an integrated methodology. Its four specific objectives are:

i. To characterize the lithological and structural framework of the Waru–Apo area through geological mapping and petrographic thin-section analysis;
ii. To assess groundwater hydrochemistry, soil geochemistry, and heavy metal concentrations using AAS and XRF analytical techniques;
iii. To evaluate groundwater pollution severity using Contamination Factor (CF), Pollution Load Index (PLI), and Nemerow's Pollution Index (NPI); and
iv. To discuss the environmental and public health implications of the findings, with specific reference to the soil–groundwater contamination linkage confirmed by Pearson correlation analysis.

2. Materials and Methods

2.1. Study Area

The Waru–Apo study area occupies the southern urban fringe of Abuja FCT, covering approximately 54.75 km² of undulating Precambrian basement terrain on the Gwagwa plains. The area is bounded by latitudes 8°54'0"N to 8°56'0"N and longitudes 7°28'0"E to 7°32'0"E. It is underlain by migmatite, granite gneiss, biotite gneiss, and anatectic granite, all products of the Pan-African orogeny (~600 Ma). The climate is tropical with a wet season (April–October) and a dry season (November–March), a seasonality that directly influences groundwater recharge rates and the dilution of heavy metal concentrations in shallow wells. Drainage is dendritic, flowing generally southeastward toward the Usuma River system, with drainage alignment controlled by the dominant NE–SW and NW–SE fracture sets inherited from the Pan-African deformation.

The conceptual hydrogeological model underpinning this study is a three-tier pathway: (1) surface source inputs — both geogenic weathering products and anthropogenic abattoir-derived contaminants introduced at the land surface; (2) vadose zone transport, mediated by soil pH, cation exchange capacity, and rainfall-driven percolation; and (3) accumulation within the fractured basement aquifer, where short residence times and minimal matrix retardation allow rapid lateral transport of dissolved metals in the direction of the regional hydraulic gradient. This framework justifies rainy-season sampling as the methodologically appropriate timing for peak contamination assessment, since wet-season dilution would understate the chronic exposure burden, and identifies the soil–groundwater interface as the critical monitoring boundary for adaptive management.

2.2. Geological and Petrographic Analysis

Systematic geological mapping was conducted across the study area at 1:25,000 scale between July and September 2020, using a Brunton compass-clinometer for structural measurements, GPS for coordinate recording, and ArcGIS 10.8 for geological map compilation (Figure 1). Representative rock samples collected from fresh outcrops across all four lithological units were prepared as petrographic thin sections (~30 µm) and examined at the Department of Applied Geology, Abubakar Tafawa Balewa University, Bauchi, under both plane-polarized (PPL) and cross-polarized (XPL) light to identify mineral assemblages, textural features, deformation microstructures, and alteration phases relevant to groundwater chemistry.

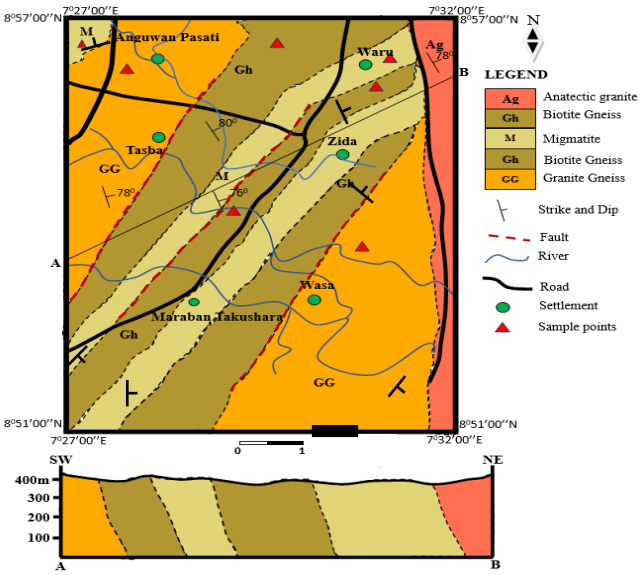

Figure 1 Geological map of Waru area

2.3. Sample Collection

Twenty-two groundwater samples were collected from eleven locations distributed across the study area: hand-dug wells, boreholes, and the seasonal stream that drains the abattoir compound and its environs (Figure 2).

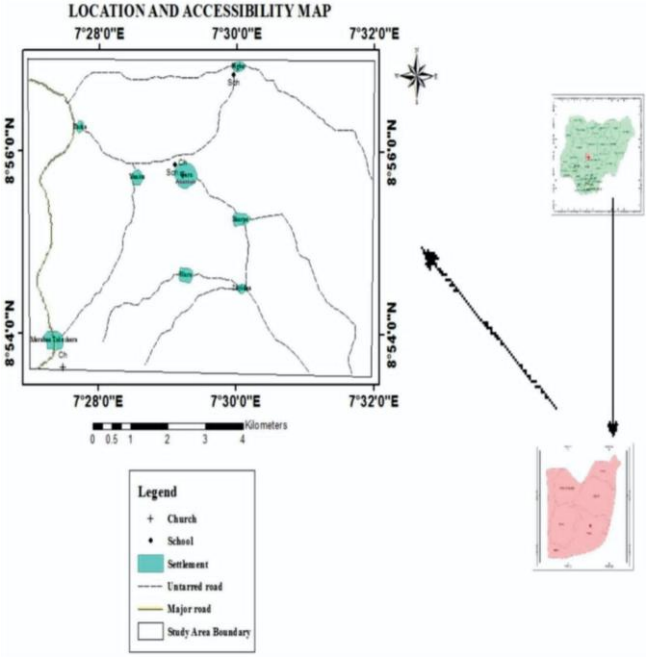

Figure 2 Location and Accessibility Map of Waru abattoir and its environs.

Eleven samples were designated for anion determination and eleven for cation and heavy metal analysis. Sampling was conducted between 8 am and 11 am during the rainy season (in the month of August, 2020), when groundwater levels are near their seasonal minimum and heavy metal concentrations reflect maximum enrichment conditions undiminished by wet-season dilution effects. The choice of wet-season sampling is a deliberate methodological decision to capture peak contamination; wet-season concentrations are expected to be lower due to dilution. This represents a conservative exposure assessment and a limitation that seasonal follow-up

monitoring would address. Ten soil samples (SS001–SS010) were collected at 0–30 cm depth along a topographic transect traversing the abattoir compound and extending downslope to document any directional enrichment pattern.

2.4. Laboratory Analysis

Field measurements of pH, temperature (T), electrical conductivity (EC), and total dissolved solids (TDS) were recorded on site using a calibrated multiparameter probe. Major cations and anions were determined at the Chemistry Department, Abubakar Tatari Ali Polytechnic, Bauchi: Na^+ and K^+ by flame photometry; Ca^{2+} and Mg^{2+} by EDTA complexometric titration (APHA [15], Method 3500); SO_4^{2-} by barium sulphate turbidimetry (Method 4500-SO4 E); HCO_3^- by acid-base titration (Method 2320 B); Cl^- by argentometric titration (Method 4500-Cl B); NH_3 by Nesslerization (Method 4500-NH3 B); NO_3^- by UV spectrophotometry (Method 4500-NO3 B). Heavy metals (Mn, Cr, Cd, Fe, Zn, Cu, Pb) in groundwater were quantified by flame atomic absorption spectroscopy (AAS) using a Perkin-Elmer A Analyst 200 instrument; detection limits were 0.001 mg/L for Cd and Pb, 0.005 mg/L for Cr, and 0.01 mg/L for Mn, Fe, Zn, and Cu. Soil heavy metals were determined by XRF spectrometry at Gombe State University. All analyses used procedural blanks, duplicates, and certified reference standards, with analytical accuracy maintained within ±5%.

2.5. Pollution Indices

Three pollution indices were applied to evaluate groundwater quality. The Contamination Factor (CF) was calculated as $CF = C_{measured} / C_{background}$, where $C_{background}$ is the WHO [16] drinking water guideline value for each metal: Mn = 0.4 mg/L; Cr = 0.05 mg/L; Cd = 0.003 mg/L; Fe = 0.3 mg/L; Zn = 5 mg/L; Cu = 1 mg/L; Pb = 0.01 mg/L. The Pollution Load Index (PLI) was computed as the seventh root of the product of all seven individual CFs per sampling site [13]; PLI < 1.0 indicates that the composite metal load does not exceed the multi-metal WHO guideline product baseline. Nemerow's Pollution Index ($NPI = C_{measured} / C_{permissible}$) evaluates individual metals independently; NPI > 1 indicates exceedance of the individual guideline value, and NPI > 3 indicates severe pollution [14].

2.6. Correlation and Data Analysis

Pearson correlation coefficients were calculated between soil and groundwater concentrations of Cr, Cd, Pb, Zn, and Cu (n = 10 paired observations; degrees of freedom = 8) to empirically evaluate the soil-to-groundwater contaminant transfer pathway. Soil samples were spatially paired with the geographically nearest groundwater sampling point using a nearest-neighbor proximity criterion. Data were assessed for approximate normality before applying Pearson r; given the small sample size, results are presented with p-values and should be treated with appropriate caution. Hydrochemical facies and geochemical processes were interpreted using Schoeller, Durov, Piper [8], and Gibbs [7] diagrams. Descriptive statistics (mean, standard deviation, minimum, maximum) were computed for all hydrochemical parameters.

3. Results and Discussion

3.1. Geological and Petrographic Characteristics

Four lithological units were mapped across the study area, with gradational rather than sharp contacts between them — a field observation that points to shared petrogenetic origin rather than four independently emplaced rock bodies. Secondary porosity, and therefore aquifer transmissivity, is enhanced throughout by the NE–SW and NW–SE fracture and joint sets that post-date peak metamorphism and are consistent with the regional Pan-African structural grain of the FCT basement.

Petrographic thin section analysis reveals that the mineralogy of these four units exerts a direct and traceable influence on the hydrochemistry of the groundwater they host.

3.1.1. Migmatite

Migmatite outcrops in both the northwestern and southeastern portions of the study area (latitude 8°53'45.4"N, longitude 7°27'22.2"E). The rock is medium-grained with a well-developed leucosome–melanosome banding. Ptygmatic fold structures confirm ductile deformation during melt-assisted flow at elevated temperatures (Figure 3). Plagioclase (albite-oligoclase) shows incipient sericitization along cleavage planes, a hydrolysis reaction that releases Na^+ and Al^{3+} into pore fluids — a primary driver of the elevated sodium concentrations in groundwater (mean Na^+ = 16.67 mg/L).

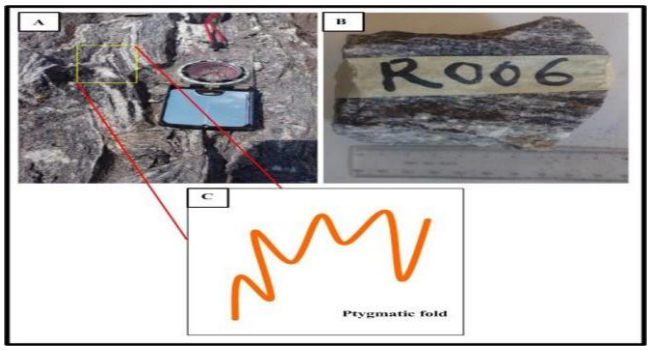

Figure 3 Photograph of an outcrop of migmatite with ptygmatic folding

3.1.2. Granite Gneiss

Granite gneiss is characterized by a foliated, medium-to-coarse-grained texture with quartz, microcline, plagioclase, and biotite as principal minerals. Biotite occurs as poikilitic crystals with brown pleochroism under PPL (Figure 4).

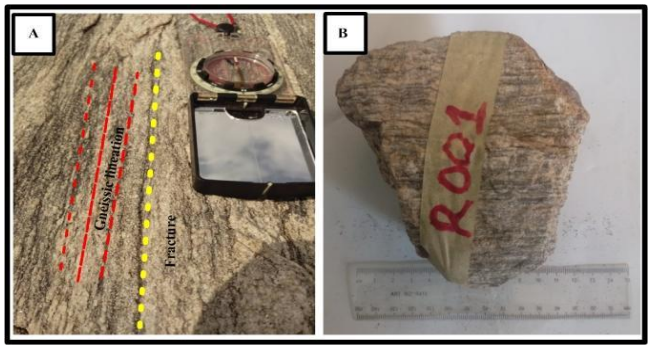

Figure 4 Field and hand Photograph of granite gneiss intruded by quartzofeldspathic

Where chloritization of biotite has occurred, Mg^{2+} and Fe^{2+} are liberated into solution, consistent with the mean groundwater Mg^{2+} of 5.11 mg/L. Quartz veins trending NE–SW and NW–SE enhance secondary permeability, deepening contaminant penetration pathways.

3.1.3. Biotite Gneiss

Biotite gneiss is the most extensive unit in the study area, exhibiting a well-developed foliation defined by alternating quartz-feldspar-rich and biotite-rich layers. Trace sulphide mineral phases — pyrite and chalcopyrite identified in thin section — are geochemically significant beyond their abundance (Figure 5). Their oxidative weathering in the unsaturated zone generates SO_4^{2-} and acidity, providing a geogenic explanation for the SO_4-dominant anion chemistry (mean SO_4 = 100.9 mg/L; Table 8) and for the low pH values recorded at several groundwater sites (minimum 5.48). Anthropogenic sulphate loading from abattoir effluent decomposition adds to this geogenic source

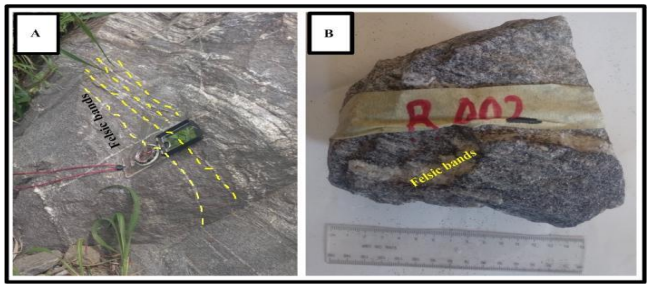

Figure 5 Field and hand Photograph of biotite gneiss intruded by quartzofeldspathic vein

3.1.4. Anatectic Granite

Anatectic granite is leucocratic and inequigranular, dominated by quartz and plagioclase with minor biotite. Plagioclase hydrolysis is the dominant source of Na^+ in the groundwater. Taken together, the petrographic evidence establishes that the Na–SO_4 and Na–Mg–SO_4 hydrochemical facies of Waru–Apo groundwater reflect plagioclase hydrolysis (Na^+ source), biotite and sulphide oxidation (SO_4^{2-} and Mg^{2+} sources), and ion exchange along fracture surfaces (Figure 6). The elevated Cr and Cd concentrations cannot be explained by rock weathering; the strong soil–groundwater correlations and spatial proximity to the abattoir confirm a dominant anthropogenic input superimposed on the geogenic baseline.

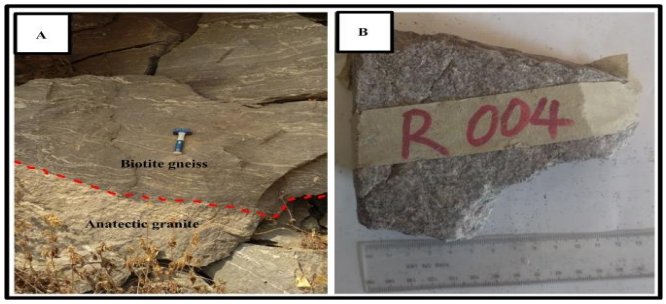

Figure 6 Field and hand Photograph of fine anatectic granite

3.2. Hydrochemical Characteristics

Groundwater pH ranged from 5.48 to 8.11 (mean 6.38), spanning moderately acidic to slightly alkaline conditions. Five of the eleven samples recorded pH below the NSDWQ lower limit of 6.5, with sample 9 reaching the minimum of 5.48. At pH 5.48, carbonate buffering is suppressed and the solubility of Cd^{2+}, Pb^{2+}, Mn^{2+}, and Zn^{2+} increases by orders of magnitude relative to neutral conditions, directly explaining the heavy metal concentrations documented in Table 3. The acidity is most plausibly generated by decomposition of abattoir organic waste — blood, viscera, bone — in the vadose zone above the water table, producing organic acids that consume the limited alkalinity of these siliceous basement soils. The abattoir waste is effectively doing duty here, supplying the cadmium itself and, through the organic acids it generates, the low-pH conditions that keep cadmium dissolved and mobile.

TDS ranged from 15 to 106 mg/L (mean 64 mg/L), and EC from 33 to 211 µS/cm (mean 132 µS/cm) — both well within WHO [16] and NSDWQ [17] permissible limits and consistent with short groundwater residence times in a fracture-dominated system. Temperature values of 24–27°C are typical of shallow basement aquifers in north-central Nigeria. Table 1 summarizes all physical parameter data of groundwater from the Waru area with statistical descriptors and WHO [16] / NSDWQ [17] standards.

Table 1 Physical parameters of groundwater samples from the Waru–Apo area

S/N	pH	TDS (mg/L)	Temp (°C)	EC (µS/cm)	Sample Type
1	8.11	62	24	132	Stream (abattoir-proximal)
2	7.40	72	27	154	Hand-dug well (abattoir-proximal)
3	6.20	15	26	33	Borehole (abattoir-proximal)
4	5.56	36	27	78	Hand-dug well (residential)
5	5.60	66	27	137	Hand-dug well (residential)
6	6.14	92	26	195	Hand-dug well (residential)
7	6.36	33	25	66	Borehole
8	6.20	52	27	104	Borehole
9	5.48	100	27	200	Borehole
10	6.86	106	27	211	Seasonal stream
11	6.30	70	26	138	
Mean	6.38	64	26.3	131.6	
Std Dev	0.805	28.7	1.009	57.6	
Min	5.48	15	24	33	
Max	8.11	106	27	211	
WHO (2017)	6.5–8.5	1000	25	2500	
NSDWQ (2007)	6.5–8.5	500	–	1000	

3.3. Soil and Groundwater Heavy Metal Concentrations

The cation order $Na^+ > Mg^{2+} > Ca^{2+}$ and anion order $SO_4^{2-} > HCO_3^- > Cl^-$, confirmed by the Schoeller plot, reflects the mineralogical weathering sequence established petrographically. Sodium concentrations ranged from 11.51 to 19.63 mg/L (mean 16.67 mg/L), well within WHO [16] limits. Sulphate ranged from 66 to 151 mg/L (mean 100.9 mg/L), approaching the NSDWQ [17] limit of 100 mg/L at the upper end. Chloride was uniformly low (1.0–2.56 mg/L), confirming negligible evaporite input. Ammonia (0.79–2.64

mg/L; mean 1.71 mg/L) exceeded the NSDWQ limit of 1 mg/L at three sites — a direct indicator of nitrogenous organic contamination linked to the decomposition of blood and offal in the soil zone above the aquifer.

Soil trace element concentrations (Table 2) increase monotonically from SS001 (the upslope control site) to SS010 (the most distal downslope sample), a directional pattern inconsistent with lithological variation in a geologically homogeneous basement terrain and pointing instead to a mobile surface source driving downslope enrichment. Chromium concentrations range from 64.1 to 842 ppm; SS007 (842 ppm) and SS008 (433 ppm) are located within approximately 50 m of the abattoir waste disposal zone, representing enrichment factors of approximately 16 and 8 times the mean rock Cr background of ~52 ppm. Lead was detected in seven of ten samples at 3.09–9.8 ppm, with the highest value at SS008, consistent with vehicle tyre combustion residues from carcass-singeing practices documented during fieldwork.

Table 2 Soil geochemical analysis results (ppm). <LOQ = below limit of quantification

Element	Cr	Pb	Cd	Zn	Cu	Ni	V	S
SS001	257	3.77	0.034	36.6	17.6	30.3	231	177
SS002	295	<LOQ	0.045	31.3	29.6	45.4	414	203
SS003	165	4.72	<LOQ	31.9	27	45.1	364	184
SS004	120	6.09	<LOQ	31.3	20.5	53.8	294	119
SS005	64.1	3.09	<LOQ	20.3	<LOQ	20.5	171	192
SS006	106	<LOQ	<LOQ	27.7	23.6	36.1	283	273
SS007	842	7.89	<LOQ	62.5	30.2	33.2	320	272
SS008	433	9.8	<LOQ	46.9	38.5	61.4	636	352
SS009	102	<LOQ	<LOQ	40	<LOQ	40.3	293	208
SS010	206	4.39	<LOQ	155	33.7	45.3	280	457

In groundwater, cadmium is the priority contaminant. Concentrations across all eleven samples (0.034–0.121 mg/L) exceed the WHO [16] and NSDWQ [17] permissible limit of 0.003 mg/L at every site, with exceedances of 11 to 40 times (Table 3).

Table 3 Heavy metal concentrations in groundwater (mg/L). S/N 1–3 = hand-dug wells (abattoir-proximal); S/N 4–6 = hand-dug wells (residential); S/N 7–9 = boreholes; S/N 10–11 = seasonal stream

S/N	Mn	Cr	Cd	Fe	Zn	Cu	Pb
1	0.055	0.046	0.096	0.121	0.026	0.009	0.005
2	0.080	0.179	0.087	0.018	0.043	0.006	0.006
3	0.129	0.114	0.041	0.013	0.121	0.012	0.007
4	0.014	0.054	0.067	0.007	0.075	0.023	0.009
5	0.031	0.077	0.063	0.022	0.041	0.013	0.003
6	0.099	0.095	0.040	0.040	0.062	0.037	0.017
7	0.053	0.049	0.079	0.015	0.079	0.037	0.023
8	0.032	0.048	0.121	0.004	0.257	0.007	0.007
9	0.045	0.075	0.034	0.005	0.039	0.007	0.019
10	0.033	0.236	0.053	0.019	0.038	0.013	0.003
11	0.135	0.077	0.115	0.006	0.092	0.009	0.004
Mean	0.064	0.095	0.072	0.025	0.079	0.016	0.009
Std Dev	0.038	0.057	0.030	0.034	0.065	0.012	0.007
Min	0.014	0.046	0.034	0.004	0.026	0.006	0.003
Max	0.135	0.236	0.121	0.121	0.257	0.037	0.023
WHO (2017)	0.4	0.05	0.003	0.3	5	1	0.01
NSDWQ (2007)	0.2	0.05	0.003	0.3	3	1	0.01

Not one site in the study area returns a compliant cadmium result, which rules out localized source proximity as the explanation: the entire shallow aquifer accessible to the community is contaminated. Chromium (0.046–0.236 mg/L) exceeded the 0.05 mg/L limit at four sites, with the maximum of 0.236 mg/L at sample 10. Lead (0.003–0.023 mg/L) exceeded the 0.01 mg/L limit at four sites, with the maximum of 0.023 mg/L at sample 7. Manganese, iron, zinc, and copper all remained within guideline values across all eleven samples.

Table 4 Soil–groundwater Pearson correlation analysis

Metal	Soil–GW Correlation (r)	p-value	Interpretation
Cr	0.82	0.003	Strong positive correlation
Cd	0.74	0.012	Moderate positive correlation
Pb	0.65	0.031	Moderate positive correlation
Zn	0.40	0.18	Weak correlation
Cu	0.55	0.08	Weak–moderate correlation

The Pearson correlation analysis (Table 4) provides the statistical link between the soil enrichment pattern and the groundwater contamination. Chromium shows the strongest soil–groundwater correlation ($r = 0.82$, $p = 0.003$), confirming that the spatial distribution of groundwater Cr closely tracks the Cr-enriched soil zone centered on the abattoir compound. Moderate correlations for cadmium ($r = 0.74$, $p = 0.012$) and lead ($r = 0.65$, $p = 0.031$) similarly confirm soil leaching as the primary transfer mechanism. Zinc and copper show weaker correlations ($r = 0.40$ and 0.55 respectively), reflecting multiple competing geochemical controls on their mobility.

3.4. Pollution Indices

The CF quantifies individual metal enrichment relative to the drinking water standard. CF values for all metals except Cd are below 1.0 at all sites, reflecting acceptable concentrations for Mn, Fe, Zn, Cu, and Pb when considered against their respective guidelines in isolation.

The Pollution Load Index (PLI) ranges from 0.001 to 0.002 across all eleven sites — all below the PLI = 1.0 threshold. This result requires careful interpretation: PLI below 1.0 does not mean the water is safe. It is a mathematical artefact of the PLI formula, where extremely low CF values for non-problematic metals dilute the signal from severely contaminated ones. A PLI of 0.001 does not mean the site is safe when cadmium alone sits at 40 times its guideline; the geometric mean simply cannot register contamination that is concentrated in a single metal.

Nemerow's Pollution Index (NPI) resolves this by evaluating each metal against its own guideline independently. NPI values for cadmium range from 11.3 (sample 9) to 40.3 (sample 8), classifying every one of the eleven sites as severely polluted for cadmium (NPI > 3). Chromium NPI ranges from 0.92 to 4.72; four sites exceed NPI = 3 (severely polluted). Lead NPI ranges from 0.3 to 2.3, with four sites exceeding the pollution threshold. Table 5, Table 6, and Table 7 present the complete CF, PLI, and NPI datasets.

Table 5 Contamination Factor (CF = C_measured / C_background; C_background = WHO [16] guideline)

S/N	Mn	Cr	Cd	Fe	Zn	Cu	Pb
1	0.138	0.92	320	0.403	0.052	0.009	0.5
2	0.2	3.58	290	0.06	0.086	0.006	0.6
3	0.323	2.28	136.67	0.043	0.242	0.012	0.7
4	0.035	1.08	223.33	0.023	0.15	0.023	0.9
5	0.078	1.54	210	0.073	0.082	0.013	0.3
6	0.248	1.9	133.33	0.133	0.124	0.037	1.7
7	0.133	0.98	263.33	0.05	0.158	0.037	2.3
8	0.08	0.96	403.33	0.013	0.514	0.007	0.7
9	0.113	1.5	113.33	0.017	0.078	0.007	1.9
10	0.083	4.72	176.67	0.063	0.076	0.013	0.3
11	0.338	1.54	383.33	0.02	0.184	0.009	0.4

* All values are 10^{-3}

Table 6 Pollution Load Index (PLI) per sampling site

S/N	Value
1	0.001374
2	0.001376
3	0.001550
4	0.001058
5	0.001052
6	0.002062
7	0.001776
8	0.001141
9	0.000969
10	0.001177
11	0.001303

Table 7 Nemerow's Pollution Index (NPI = C_measured / C_permissible) per metal and site

S/N	Mn	Cd	Cr	Cu	Fe	Pb	Zn
1	0.138	32.0	0.920	0.009	0.403	0.500	0.005
2	0.200	29.0	3.580	0.006	0.060	0.600	0.009
3	0.323	13.7	2.280	0.012	0.043	0.700	0.024
4	0.035	22.3	1.080	0.023	0.023	0.900	0.015
5	0.078	21.0	1.540	0.013	0.073	0.300	0.008
6	0.248	13.3	1.900	0.037	0.133	1.700	0.012
7	0.133	26.3	0.980	0.037	0.050	2.300	0.016
8	0.080	40.3	0.960	0.007	0.013	0.700	0.051
9	0.113	11.3	1.500	0.007	0.017	1.900	0.008
10	0.083	17.7	4.720	0.013	0.063	0.300	0.008
11	0.338	38.3	1.540	0.009	0.020	0.400	0.018
Mean	0.161	24.1	1.911	0.016	0.082	0.936	0.016
Max	0.338	40.3	4.720	0.037	0.403	2.300	0.051
Min	0.035	11.3	0.920	0.006	0.013	0.300	0.005

3.5. Hydrogeochemical Processes

The Gibbs [7] diagram places all eleven groundwater samples in the rock weathering dominance field. Intermediate TDS and Na/(Na+Ca) values confirm that silicate mineral dissolution rather than evaporative concentration or direct rainfall input is the primary control on major ion chemistry. Two samples with the highest TDS values show a marginal shift toward the evaporation pole, suggesting slightly longer water–rock contact times in deeper fracture zones. No samples plot in the atmospheric precipitation field.

The Durov plot places the majority of samples in field 2, indicating significant cation exchange: Ca^{2+} and Mg^{2+} are being replaced by Na^{+} on secondary clay mineral surfaces formed from feldspar weathering, consistent with the petrographic observation of sericitized plagioclase in the migmatite and granite gneiss. Samples in field 5 represent recently recharged, geochemically immature groundwater — the most vulnerable to surface-introduced contamination. The Schoeller diagram confirms the cation and anion ordering established from the raw data, while the Piper plot identifies the two water types — Na–SO_4 and Na–Mg–SO_4 — that reflect the mineralogical weathering sequence described petrographically. The combined picture is one of a rock-weathering-dominated hydrochemical system operating under progressive anthropogenic stress: major ion composition is explainable from first principles of basement rock mineralogy; the heavy metal composition is not. Major ion data are presented in Table 8.

Table 8 Cation and anion concentrations in groundwater (mg/L)

S/N	Na	Ca	Mg	NH_3	Cl	SO_4	NO_3
1	13.97	0.362	3.455	1.12	1.03	109	8
2	15.57	0.288	3.771	1.68	1.10	104	7
3	19.45	3.678	9.755	1.90	1.16	66	9
4	18.91	0.878	5.626	2.27	1.76	83	5
5	11.51	0.027	1.933	2.64	1.13	75	6
6	15.93	0.967	5.354	1.49	1.00	93	8
7	17.42	0.272	3.548	0.79	1.30	88	4
8	15.83	0.823	6.199	2.24	1.56	102	6
9	18.63	1.409	4.882	1.68	2.00	107	5
10	19.63	0.249	3.411	1.91	1.00	132	7
11	16.56	1.267	8.313	1.12	2.56	151	8
Mean	16.67	0.929	5.113	1.713	1.418	100.9	6.6
WHO (2017)	200	150	50	3	250	250	50
NSDWQ (2007)	200	–	20	1	250	100	50

Elevated Cr, Cd, and Pb indicate additional anthropogenic contributions, empirically linked to soil contamination.

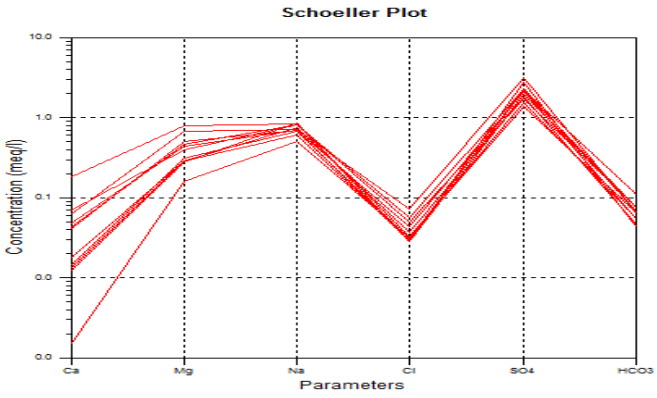

Figure 7 Schoeller diagram of ionic composition

Schoeller plot shows the average chemical composition of the groundwater samples in the area (Figure 7). The relative

trend for the cations shows that Na > Mg > Ca, and that of the anions showed that SO_4> HCO_3> Cl.

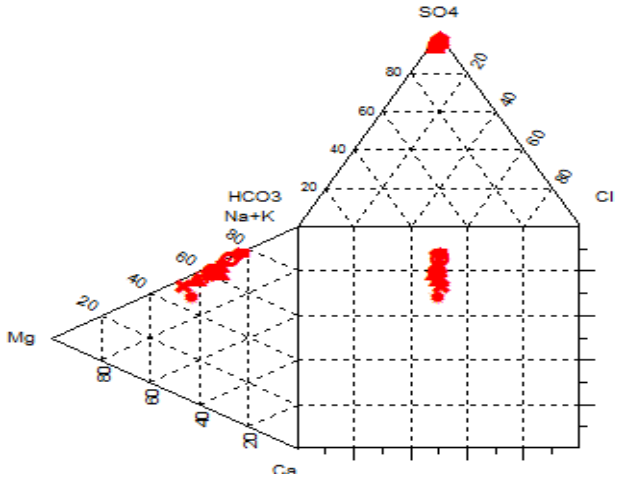

Figure 8 Durov plot of major ions in the water samples

The Durov plot shows that the water samples collected for the study plot in fields 2 and 5, with majority of the samples plotting in field 2 (Figure 8). Water samples in field 2 indicate an important ion exchange (with significant sodium ions). Samples in field 5 indicate fresh recent recharge water exhibiting simple dissolution or mixing.

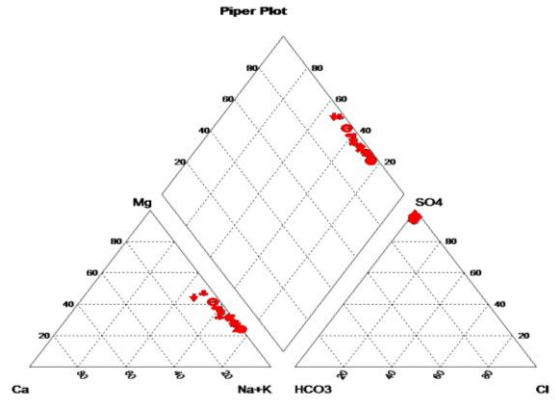

Figure 9 Piper plot showing hydrochemical facies

The hydrochemical analysis revealed two water types namely Na-SO_4 water type; and Na-Mg-SO_4 water type as obtained from Piper plot (Figure 9).

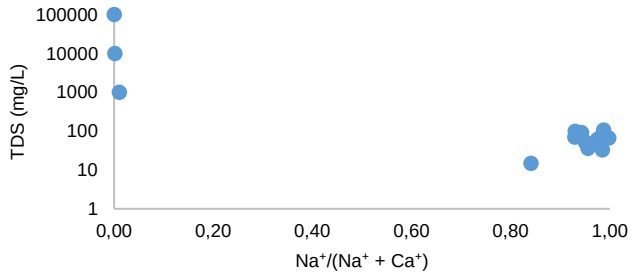

Figure 10 Gibbs plot

Gibbs [7] plot given in Figure 10 shows the distribution of the water sample points in Waru and its environs by majorly in the central part of the plot. The central location of the water sample points shows dominance weathering of rocks in controlling the geochemistry of water in Waru and its environs.

3.6. Environmental and Health Implications

The data assembled in this study describe a groundwater contamination crisis that is already affecting the Waru–Apo community. Cadmium at 0.034–0.121 mg/L in every one of the eleven sampled wells and boreholes means that every resident drawing domestic water from a shallow source in this study area is being chronically exposed to cadmium at concentrations between 11 and 40 times the safe drinking water guideline. Chronic cadmium exposure at these concentrations is associated in the epidemiological literature with renal tubular dysfunction, progressive osteoporosis (Itai-itai syndrome), and statistically elevated risk of lung and endometrial cancers [16]. It crosses the placental barrier and accumulates in developing fetal renal tissue, making pregnant women and unborn children particularly vulnerable. Children under five who consume contaminated water face developmental risks that will not be immediately visible but will manifest in impaired renal function and bone density deficits in adulthood (Table 9).

The four sites where chromium exceeds its 0.05 mg/L guideline (with a maximum of 0.236 mg/L at sample 10) add a carcinogenic dimension to the exposure burden. Chromium speciation was not determined in this study; however, the combination of variable oxidizing conditions and anthropogenic Cr loading from abattoir waste suggests that a proportion of the dissolved chromium may be present in the hexavalent form (Cr^{6+}), associated with lung cancer and gastrointestinal tract damage upon chronic ingestion. The precautionary principle warrants treating these sites as potentially containing Cr^{6+} until speciation data are available. Lead exceedances at four sites (maximum 0.023 mg/L at sample 7) are particularly concerning for children, given that lead's neurotoxic effects on cognitive development have no established threshold.

Table 9 WHO [16] and NSDWQ [17] drinking water standards and health effects

Parameter (mg/L)	NSDWQ (2007)	WHO (2017)	Health Impact
Cadmium	0.003	0.003	Nephrotoxic; kidney damage; carcinogenic
Chromium	0.05	0.05	Carcinogenic (Cr^{6+}); gastrointestinal damage
Lead	0.01	0.01	Neurotoxic; cognitive impairment in children
Manganese	0.20	0.40	Neurological disorder
Iron	0.30	0.30	Aesthetic; no direct health threshold
Zinc	3.00	5.00	Gastro-intestinal disorder at high doses
Copper	1.00	2.00	Gastro-intestinal disorder
pH	6.5–8.5	6.5–8.5	Corrosion at low pH; metal mobilisation
TDS	500	1000	Aesthetic; no direct health threshold
Sulphate	100	250	Laxative effects at high doses
Nitrate	50	50	Cyanosis; methemoglobinemia in infants
Ammonia	1.00	1.50	Indicator of faecal contamination

The soil–groundwater correlation analysis confirms that the contamination mechanism is ongoing and dynamic: surface contaminants leach downward through the vadose zone

during rainfall events, driven by the hydraulic gradient and facilitated by acidic soil conditions that suppress metal adsorption onto soil particle surfaces. Wet-season concentrations in the shallow wells are likely to exceed the dry-season values documented in this study, as recharge pulses mobilize freshly deposited contaminants from the abattoir surface.

4. Conclusion

The Waru–Apo area presents a convergence of geological conditions and land-use practices that together create a groundwater contamination scenario that is both scientifically tractable and practically urgent. The fractured crystalline basement with migmatite, granite gneiss, biotite gneiss, and anatectic granite provides an aquifer whose hydrochemistry is predictably governed by plagioclase hydrolysis, biotite and sulphide oxidation, and ion exchange along fracture surfaces, producing the Na–SO_4 and Na–Mg–SO_4 water types confirmed by Gibbs, Durov, Schoeller, and Piper diagram analysis. The same fractures that give the community its only access to water also carry surface contaminants down to the water table with little to no retardation.

The contamination signal documented in this study is severe by any measure. Cadmium exceeds the WHO [16] and NSDWQ [17] permissible limit of 0.003 mg/L at all eleven groundwater sampling sites, with NPI values of 11.3 to 40.3 classifying every site as severely polluted for cadmium alone. Chromium exceeds its guideline at four sites (NPI up to 4.72) and lead at four sites (NPI up to 2.3). The soil–groundwater Pearson correlations (Cr $r = 0.82$; Cd $r = 0.74$; Pb $r = 0.65$) establish that the dominant transfer mechanism is soil leaching: abattoir-derived surface contaminants are moving through the vadose zone into the shallow aquifer, driven by gravity, precipitation, and the acidic soil conditions that maximize heavy metal solubility. Every one of the eleven sites shows the same pattern, so this is not a localized hotspot but a systemic, area-wide impairment of the aquifer serving the Waru–Apo community.

The findings have immediate implications for water resource management in this part of the FCT. Routine quarterly monitoring of Cd, Cr, and Pb in shallow groundwater is necessary as a minimum public health safeguard. Enforcement of abattoir effluent containment under existing NESREA and FCTEPB regulations must be prioritized to arrest further soil loading. Community-scale point-of-use treatment and the provision of deeper boreholes below the contaminated regolith represent the most practicable near-term interventions. Future research should extend this framework to include seasonal concentration variability, formal health risk assessment using Hazard Quotient and carcinogenic risk indices for the specific exposure pathways of the Waru–Apo population, and principal component analysis to definitively partition geogenic and anthropogenic contributions to the observed metal loads.

Recommendations

- Hydrogeological Monitoring: Establish a quarterly groundwater quality monitoring program for Cd, Cr, and Pb at all eleven sites documented in this study, with dry-season (March–April) sampling treated as the highest priority given minimum dilution conditions. Results should be reported to the FCT Environmental Protection Board and Abuja Municipal Area Council on a bi-annual basis.
- Pollution Control: The Waru abattoir operators, FCTEPB, and AMAC should jointly implement impermeable drainage channels, effluent settlement and treatment facilities, and a ban on the discharge of blood, offal, and wash water onto open ground. These measures should be enforced under existing NESREA regulations before the next wet season.
- Water Supply Intervention: New community boreholes targeting fracture intersections at depths greater than 30 m should be drilled using the structural data from this study as a siting guide. Electrical resistivity tomography surveys should precede drilling. Residents within 500 m of the abattoir should be provided with point-of-use treatment — activated carbon or reverse osmosis — as an immediate protective measure.
- Public Health and Research: Community awareness programs on the health risks of cadmium and chromium exposure should be conducted in collaboration with the FCT Primary Health Care Development Agency. Interdisciplinary research integrating hydrogeology, public health, and environmental law is needed to develop a comprehensive contamination management framework for the Waru–Apo area and analogous basement terrains across the FCT.

Author Contributions

HAB: Conceptualization, Investigation, Methodology, Data Curation, Formal Analysis, Visualization, Writing-Original Draft, Writing – Review & Editing; **BSJ:** Data Curation, Formal Analysis, Writing-Original Draft; **IYT:** Formal Analysis, Writing – Review & Editing, Supervision; **AS:** Investigation, Methodology, Writing-Original Draft

Conflict of Interest

The authors have no conflicts of interest to declare.

References

[1] Freeze RA, Cherry JA. *Groundwater*. Englewood Cliffs, N.J.: Prentice-Hall (1979). 604 p.

[2] Fetter CW. *Applied hydrogeology*. Upper Saddle River, NJ: Prentice Hall (2001). 598 p.

[3] Emenike PC, Nnaji CC, Tenebe IT. Assessment of geospatial and hydrochemical interactions of groundwater quality, southwestern Nigeria. *Environmental Monitoring and Assessment* (2018) **190**(7):440. doi:10.1007/s10661-018-6799-8.

[4] Elemile OO, Raphael DO, Omole DO, Oloruntoba EO, Ajayi EO, Ohwavborua NA. Assessment of the impact of abattoir effluent on the quality of groundwater in a residential area of Omu-Aran, Nigeria. *Environmental Sciences Europe* (2019) **31**(1):16. doi:10.1186/s12302-019-0201-5.

[5] Alloway BJ, editor. *Heavy metals in soils: Trace metals and metalloids in soils and their bioavailability*. Dordrecht, LaVergne, Tenn.: Springer Netherlands; MyiLibrary (2013).

[6] Reimann C, Caritat P de. Distinguishing between natural and anthropogenic sources for elements in the environment: regional geochemical surveys versus enrichment factors. *The Science of the total environment* (2005) **337**(1-3):91–107. doi:10.1016/j.scitotenv.2004.06.011.
[7] Gibbs RJ. Mechanisms controlling world water chemistry. *Science (New York, N.Y.)* (1970) **170**(3962):1088–1090. doi:10.1126/science.170.3962.1088.
[8] am Piper. A graphic procedure in the geochemical interpretation of water-analyses. *Eos, Transactions American Geophysical Union* (1944) **25**(6):914–928. doi:10.1029/TR025i006p00914.
[9] Mehdi M, Hakim, Djafer Khodja, Amina, Aichour, Naourredine G. Multivariate statistical analysis of groundwater quality of Hassi R'mel, Algeria. *Journal of Ecological Engineering* (2023) **24**(5):22–31. doi:10.12911/22998993/161140.
[10] Afolabi AO, Adenigba VO, Adeboye AC, Akinwole IO, Amos DD, Adegboye HO, et al. Hydrogeochemistry and microbial diversity assessment of anthropogenic activities on a suburban ecosystem within Ibadan, SW Nigeria. *Environmental Monitoring and Assessment* (2026) **198**(5):517. doi:10.1007/s10661-026-15344-8.
[11] Appelo CA, Postma D. *Geochemistry, groundwater and pollution*. Leiden: A.A. Balkema Publishers (2005). 615 p.
[12] Hem JD. *Study and interpretation of the chemical characteristics of natural water*. Washington, D.C.: U.S. Gov. Print. Off (1985). 263 p.
[13] Tomlinson DL, Wilson JG, Harris CR, Jeffrey DW. Problems in the assessment of heavy-metal levels in estuaries and the formation of a pollution index. *Helgoländer Meeresuntersuchungen* (1980) **33**(1-4):566–575. doi:10.1007/BF02414780.
[14] Boateng TK, Opoku F, Acquaah SO, Akoto O. Groundwater quality assessment using statistical approach and water quality index in Ejisu-Juaben Municipality, Ghana. *Environmental Earth Sciences* (2016) **75**(6):489. doi:10.1007/s12665-015-5105-0.
[15] APHA. *Standard Methods for the Examination of Water and Wastewater* **APHA, AWWA, WEF**. Washington, DC: American Public Health Association (2005).
[16] WHO. *Guidelines for drinking-water quality*. Geneva: World Health Organization (2017). 541 p.
[17] Standards Organisation of Nigeria. *Nigerian Standard for Drinking Water Quality* **NIS 554:2007**. Abuja: Standards Organisation of Nigeria (2007).